Detailed design and optimization of ferroelectric tuners

Ilan Ben-Zvi,[1,*] Alick Macpherson,[2,†] and Samuel Smith[2,‡]

[1]*Physics and Astronomy Department, Stony Brook University, Stony Brook, New York 11794-3800, USA*
[2]*CERN, CH-1211 Geneva, Switzerland*

(Received 29 April 2025; accepted 16 July 2025; published 10 September 2025)

A detailed, step-by-step design methodology of a ferroelectric fast reactive tuner (FE-FRT) capable of modulating Mega VAR reactive powers on a submicrosecond timescale is given. Closed expressions of values for all the components of the tuner are detailed, and tuner performance optimization is addressed, resulting in a figure of merit measure of FE-FRT tuner performance and use case applicability over a wide range of rf frequencies and reactive power levels. This enables addressing feasibility and rapid assessment of design parameters given an FE-FRT tuning scenario defined by required tuning range, cavity operating frequency, and cavity stored energy.

DOI: 10.1103/9sf7-wwyb

I. INTRODUCTION

Frequency tuning of accelerator cavities is a fundamental tool of accelerator science and technology. The ferroelectric fast reactive tuner (FE-FRT) extends the capability of tuners toward faster and higher-power tuning for both normal conducting and superconducting cavities.

Recent work on ferroelectric tuners and related technologies indicates a growth in the applications of cavity tuners [1–4] and related applications of ferroelectric phase shifters [5,6].

This communication extends the previously developed [7,8] theory and methodology of high-power FE-FRTs, adds a detailed, step-by-step design procedure for such an FE-FRT device, and provides methods for optimizing its performance across a broad range of rf frequencies and reactive power levels. Finally, the reader is guided through the electromagnetic simulation procedure, so as to permit comparison between the analytic model and electromagnetic design.

In addition to the presentation of the FE-FRT design process, one of the main conclusions of this work is the design advantages gained from FE-FRT tuner designs comprising just two ferroelectric wafer elements. Given the challenge of designing high average power tuners, where power dissipation in the ferroelectric material is a central design driver, the interplay between power handling capability and the rf design is what is developed in this paper, in terms of FE-FRT applicability and tuner performance reach. The rationale for key design choices to determine optimum tuner parameters compliant with given frequency and tuning power requirements is given and is followed by a comparison of analytical results with detailed numerical simulation of several challenging high-power tuner scenarios. The comparisons show that analytical expressions evaluated using Maple [9] closely approximate results obtained with CST's Studio suites' finite element solver [10], giving credence to the underlying design methodology.

A. Methodology

When tasked with designing a high-power tuner, the typical input constraints are (i) The cavity resonant frequency, f_0, $\omega_0 \equiv 2\pi f_0$. (ii) The required tuning range, Δf. (iii) The stored energy of the cavity, U.

The tuner can be considered an impedance at the port of the cavity to be tuned, with the complex power P flowing from the cavity to the tuner. With this view, the real part of this complex power is dissipated power in the tuner, which has to be accommodated for in its design. This dissipated power should be kept low so that the thermal management of the tuner is less demanding, and to also reduce undesirable rf power drainage from the cavity, which would otherwise need to be replenished by the rf drive. The imaginary part of P is the reactive power flowing into the tuner and is responsible for the frequency tuning of the cavity. For a tuning range (lowest and highest frequency) defined by "tuner end states" and described with subscripts 1 and 2, the product of the stored energy and the required tuning range determines the reactive power that has to flow from the cavity to the tuner [7]:

$$\Im(\Delta P_{12}) = 2U\Delta\omega_{12}. \tag{1}$$

*Contact author: Ilan.Ben-Zvi@StonyBrook.edu
†Contact author: alick.macpherson@cern.ch
‡Contact author: samuel.jack.smith@cern.ch

For demanding tuner design requirements, a large reactive power is to be foreseen, and this, in turn, can imply additional engineering considerations to the design, in order to avoid issues such as rf voltage breakdown thresholds at the coupler port, transmission line, or tuner body.

The FOM represents the maximal change in reactive power per the average dissipated power in the tuner system and is a clear performance indicator for the tuner. The FOM can be presented in terms of the reactance X (used for the frequency tuning) to the resistance R (wasted dissipation) over the full tuning range, where $Z = R + jX$ is the complex impedance of the tuner at the cavity port. The FOM is given by

$$\mathrm{FOM} \equiv \frac{\Im(P_2) - \Im(P_1)}{2\sqrt{\Re(P_1)\Re(P_2)}} = \frac{X_2 - X_1}{2\sqrt{R_1 R_2}}. \tag{2}$$

Given that the reactance and resistance vary in a complex way as a function of the permittivity, the FOM, as defined, serves as a useful but approximate indicator of performance.

II. KEY DESIGN CHOICES

Until now, the details of the tuner circuit were not determined, and the tuner is simply represented by a tunable impedance at the port of the cavity. Assuming a tunable reactance achieved by a ferroelectric loaded capacitor for tuning functionality, Ref. [7] introduced a number of potential equivalent circuit designs, with both nonresonant and resonant circuit options considered.

A. The tuner as an impedance

For achieving a high FOM performance, a resonant tuner circuit with capacitive coupling to the cavity was found to be the most effective and is taken as the starting point for this work. Figure 1 gives the general equivalent circuit, where the C_f, L, R are the resonator parameters containing the ferroelectric segment, with C_S is for impedance matching of the tuner to the cavity. While the resonant frequency of the tuner circuit is set by the LC circuit,

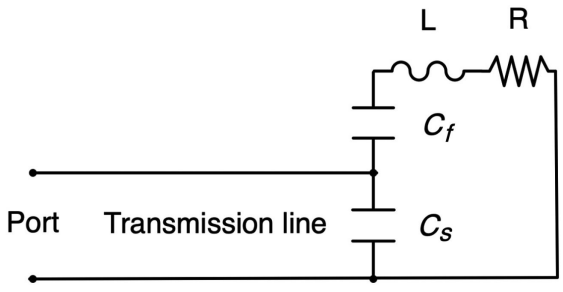

FIG. 1. The equivalent circuit of a capacitive coupled resonant tuner.

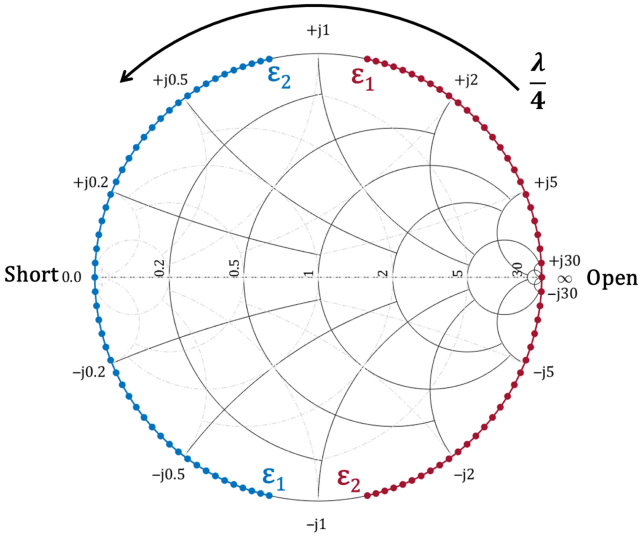

FIG. 2. Smith chart showing an example of the tuner's impedance as a function of permittivity centered around a central permittivity for just the resonator (marked in red) and for the resonator followed by a quarter-wavelength transmission line (marked in blue).

the choice of tuner inductance L can be made such that the tuning range is made symmetric around f_0, thereby minimizing the peak voltage. Also implicit in this schematic is a transmission line, with line length set at one quarter wavelength, which transforms the tuner impedance such that at the interface to the cavity, the tuner system presents an impedance that is well defined and continuous over the full tuning range—thus symmetric around the short position on the Smith chart (see Fig. 2). This configuration is appropriate for an analog tuning response.

As previously established [7], the achievable tuning range can be derived by considering the tuner as an external impedance coupled to the cavity with a transformer turn ratio given by a port impedance Z_0 and a quality factor Q_e:

$$\Delta\omega_{12} = 2\pi\Delta f_{12} = \frac{\omega_0}{2Q_e}\frac{X_2 - X_1}{Z_0}. \tag{3}$$

For a given tuning range, the ratio of the change in reactance $X_2 - X_1$ to the product $Q_e Z_0$ is determined, and in what follows, the procedure for determining the required change in reactance, $X_2 - X_1$, that maximizes the FOM is detailed.

B. The ferroelectric material

In the FE-FRT tuner, the tuning function is achieved through the application of a variable bias voltage to a ferroelectric capacitor, with the applied bias voltage inducing a change in the permittivity of the ferroelectric. This tunable permittivity implies a controllable variable reactance that can be incorporated into the resonant LC circuit of the tuner and coupled to the cavity. To realize this

ferroelectric capacitance, a flat wafer format is ideal for the ferroelectric material, as it permits a reduced bias voltage for a given polarizing electric field (small wafer thickness) and improves the thermal conductivity for cooling the wafer (larger wafer surface area). In addition, Ref. [7] demonstrated that an annular wafer geometry reduced parasitic inductance and resistance losses at the capacitor-spacer transition. As such, the ferroelectric capacitance considered here is a stack of N_w of annular wafers connected in series, with the wafers separated by copper spacers that allow both for the application of bias voltage across the ferroelectric wafers and for the provision of cooling of the wafers.

Assuming an annulus wafer geometry in a multistack assembly of ferroelectric capacitors, the total capacitance area of the wafer stack of ferroelectric capacitors is $A = N_w\pi(r_a^2 - r_i^2)$ and is the surface area over which heat can be extracted from the ferroelectric. Here, r_a and r_i, the outer and inner radii of the wafers, and the wafer thickness is g.

The tuning range is mapped to a range in relative permittivity ϵ of the ferroelectric, where ϵ is varied by applying a bias electric field across the ferroelectric capacitor, with the full tuning range mapped to a relative permittivity range, $\epsilon_1 - \epsilon_2$, defined by the tuner end states.

In terms of the current ferroelectric of choice, a BST ceramic ($BaTiO_3/SrTiO_3$-Mg) [11] is recommended, which has a room temperature of permittivity of $\sim\epsilon = 160$, and is a low loss ceramic, with a very low frequency dependent loss tangent. The typical measured loss tangent value is $\delta = 3.4 \times 10^{-4}$ at 80 MHz, and a frequency scaling of $\sim\omega^{0.783}$ between 80 and 400 MHz, depending on material temperature, has been reported [11].

A FOM for bare ferroelectric material can be derived, and as it neglects any dissipation in other elements of the tuner circuit, it represents an upper limit on the achievable FOM. This reference FOM is given by

$$\mathrm{FOM(FE)} = \frac{\Delta\epsilon}{2\delta\epsilon_c}, \tag{4}$$

where $\Delta\epsilon = |\epsilon_2 - \epsilon_1|$, and ϵ_c is a central value for the relative permittivity, approximated by $\epsilon_c \approx \sqrt{\epsilon_1\epsilon_2}$. For the aforementioned BST ceramic, this figure of merit is temperature dependent with a peak at about 50 °C. At this temperature, with permittivity end states defined by a sustainable bias electric field of up to 8 MV/m, $\epsilon_1 = 96$, $\epsilon_2 = 130$, and the frequency dependent loss tangent at 400 MHz is $\delta = 9.5 \times 10^{-4}$. This, in turn, implies a FOM(FE) = 156, which can be considered an upper limit on tuner performance. For higher-power tuner designs, Eq. (4) implies that a lower average permittivity enables an improved FOM(FE) performance reach, but may come at the cost of limiting the permittivity range, thereby limiting the tuning range.

C. Aspect ratio of the ferroelectric capacitor

Power dissipation in the ferroelectric material dominates the technical challenges of designing high-power tuners, and special attention must be given to thermal management issues, in particular, due to the increase in the loss tangent with operating frequency. Therefore, this work places the thermal management of the ferroelectric at the foundation of the tuner's design. Using the material FOM, as defined in Eq. (4), the resulting limit on the temperature increase in the ferroelectric material is given in Eq. (5), and this is then used to derive the optimal aspect ratio of the ferroelectric wafer in Eq. (6), which is mapped against frequency and power level in Fig. 3.

To understand the implications of power dissipation for the realization of the tuner's design geometry, the power dissipated in the tuner's circuit is distributed between the ferroelectric ceramic and the copper conductor elements, and must be considered separately. For a ferroelectric capacitor comprised of N_w wafers connected in series, the wafer geometry is key to optimizing the power dissipation, with the wafer area-to-thickness aspect ratio used to quantify both the ferroelectric capacitance and the thermal transport at the wafer interface. The latter is relevant, as it determines the temperature rise in the wafer that must be accommodated by a cooling system integrated into the wafer stack spacers. For example, assuming the cooling circuit provides a refrigerant at 20 °C and the ferroelectrics operating temperature is set at 50 °C, the maximum allowable average temperature increase of the ferroelectric from dissipative losses is limited to 30 °C. This limitation is not strictly necessary but represents a compromise between maximizing the FM(FE), minimizing the wafer's area, and addressing the engineering constraints of the cooling circuit. This

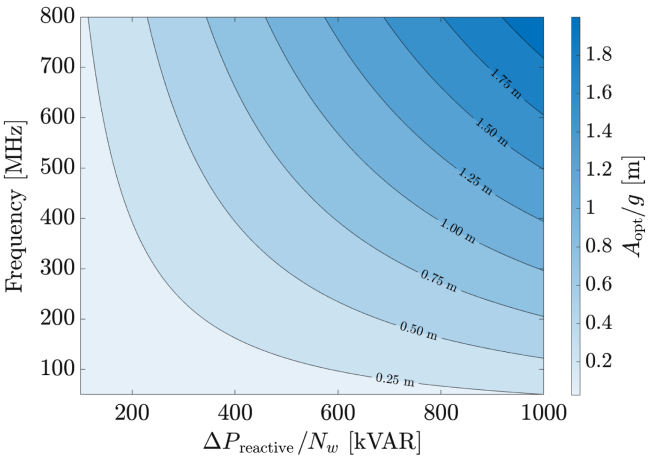

FIG. 3. The optimal ratio of a single wafer cross-sectional area to gap A_{opt}/g in meters as a function of the wafer reactive power $\Delta P_R/N_w$ in units of kVAR and operating frequency in MHz. The ferroelectric material properties are as noted in Sec. II B, and a wafer temperature rise of 30° is assumed.

is particularly relevant to the cooling circuit geometry, as for a fluid cooling system that depends on the ability to extract dissipative power from the spacers between the wafers, mechanical constraints from cooling channel dimensions must be considered; as a conservative estimate, the spacer thickness must be at least 5 mm for $N_w = 2$ or 10 mm for larger N_w to accommodate cooling lines. It is worth noting that other methods for cooling the wafers could be envisioned, but the analytic equations provided herein are independent of the specifics of the implementation details.

To determine the optimum aspect ratio of an individual wafer, with a single-face surface area of A, consider that tuner operation generates a power dissipation of P_W in the N_w wafer series-connected stack. Assuming that heat can be extracted from both faces of each wafer, and that the cooling can accommodate an average temperature rise ΔT in the wafers, then for a power flow of $P_W/2$ flowing from the wafer center to the surface area A,

$$\Delta T = \frac{2}{g}\int_0^{g/2} T(y)\,\mathrm{d}y = \frac{P_W g}{12KA}. \tag{5}$$

Here, K is the thermal conductivity of the ferroelectric material [11]. Equating this ΔT with that of the target temperature rise in the wafer relative to its cooled surface, the optimal wafer aspect ratio A_{opt}/g can be given by

$$A_{\mathrm{opt}}/g = \frac{P_W}{12\Delta TK} = \frac{\Delta P_R}{12N_w K\Delta T}\frac{\delta(\omega)\sqrt{\epsilon_1\epsilon_2}}{\Delta\epsilon}, \tag{6}$$

where $\Delta P_R = \Im(\Delta P_{12}) = 2N_w P_W$ FOM(FE) is the peak reactive power in the complete tuner. Given that the FOM improves with a reduced capacitance, this aspect ratio is considered optimal, as the wafer stack capacitance is proportional to $A/(gN_W)$. Figure 3 shows a contour plot of this optimal aspect ratio as a function of peak reactive power in a single wafer $\Delta P_R/N_w$ and cavity frequency f_0.

With an optimal ratio A_{opt}/g, the actual area and wafer thickness must be determined by engineering considerations, which are beyond the scope of this paper. However, it is noted that while the power of the bias driver of the ferroelectric capacitor varies as g^2 giving a preference for a smaller g, smaller wafer areas may increase the temperature step from the spacers to the wafers, making cooling them more difficult, and suggesting a larger value of g is preferred. As a compromise, a wafer thickness between 0.2 and 1 mm is recommended, depending on manufacturing feasibility.

III. THE RESONANT TUNER

For optimum tuner performance, the tuner equivalent circuit shown in Fig. 1 should be resonant over frequencies defined by the cavity and required tuning range, and it offers two important advantages over nonresonant designs: (i) The reactance change of the ferroelectric capacitor is amplified parametrically, yielding a reactance change in the resonator that is Q times larger, where Q is the quality factor of the resonator. (ii) By adjusting the resonator's frequency Ω_0, taken at a central value of the permittivity range and making it approximately equal to the cavity's frequency ω_0, the impedance of the resonator is made symmetric in both end states of the tuner.

In the following sections, the constraints on the LCR circuit parameters are detailed.

A. Modeling the resonator

With the LCR circuit parameters as per Fig. 1, C_f represents the ferroelectric capacitance, L, the tuner inductance including the ferroelectric capacitor and its support spacers, and $R = R_C + R_L$ is the total resistance of the circuit, comprising contributions from dielectric loss in the capacitor as well as the inductive resistance. The resonant frequency of the tuner's circuit is then $\Omega = 1/\sqrt{LC}$, where C is the total capacitance, and the resonant circuit has a shunt resistance $\mathbb{R} = Q\sqrt{L/C}$. The total tuner capacitance C is the in-parallel sum

$$C = \frac{C_s C_f}{C_s + C_f} \tag{7}$$

and given the dissipative nature of the ferroelectric capacitor, it contributes $R_C = \delta/(\Omega_0 C_f)$ to the resistivity.

To quantify the tuner inductance L for a stacked wafer geometry, the inductor may be considered a short coaxial transmission line. At low frequencies ($f_0 < 30$ MHz), the resonator can be constructed as a compact lumped element resonant circuit, but this simplification is not relevant to most tuners, so the short terminated coaxial line modeling is adopted.

To fully model the total resistance of the resonant section, the inductor loss is taken as the series sum of the resistive loss from the ferroelectric, the resistance of the short transmission line segment, and the effect of the current at the end-wall terminations of the line representation of the inductor so that

$$R = R_C + R_L = R_C + R_i + 2R_B, \tag{8}$$

where R_B is the end-wall line termination resistance of the resonator. Note that the inductor is modeled as a coaxial line terminated at both ends, so R_B appears twice in Eq. (8).

Using the standard transmission line expression for the impedance of the coaxial stacked wafer LCR resonator, the resistance contribution R_i can be determined as

$$
\begin{aligned}
Z_i &= Z_{r0}\frac{2R_B + Z_{r0}\tanh(\gamma l)}{Z_{r0} + 2R_B\tanh(\gamma l_r)} \\
&\sim 2R_B + Z_{r0}\alpha l_r(1+\tan(\beta l_r)^2) + jZ_{r0}\beta l_r \\
&= R_i + 2R_B + jX_i
\end{aligned} \tag{9}
$$

where Z_{r0} is the characteristic line impedance for the resonator, $\gamma = \alpha + j\beta$ is the complex propagation coefficient of the line, with $\beta = \Omega/c$, and $l = l_r$ is the transmission line length. From this, the resistive component R_i is

$$
R_i\tilde{Z}_{r0}\alpha l_r(1+\tan(\beta l_r)^2), \tag{10}
$$

where the approximation assumes the tuner is compact, and l_r is much shorter than the wavelength of the rf.

Here, the transmission line attenuation factor α is defined for a coaxial geometry with inner and outer conductor radii of a_r and b_r, respectively, as

$$
\alpha = \frac{R_s}{2\eta\log(\frac{b_r}{a_r})}\left(\frac{1}{a_r}+\frac{1}{b_r}\right), \tag{11}
$$

where $\eta = \sqrt{\mu_0/\epsilon_0} = 376.7\ \Omega$ is the impedance of free space, $R_S = \sqrt{\pi f\mu_0/\sigma}$ is the surface resistance, and σ is the bulk conductivity of the conductors.

Similarly, the effect of the current at the end wall of the transmission line, represented by R_B, for a standard coaxial short is given by

$$
R_B = \frac{R_S}{2\pi}\log(b_r/a_r). \tag{12}
$$

This now permits the evaluation of the impedance Z_r of the tuner section, as a capacitively coupled resonator as measured at the tap point of the transmission line, and is a series-parallel combination, with

$$
\begin{aligned}
Z_r &= \frac{Z_{C_S}(Z_{C_f}+Z_i+R)}{Z_{C_S}+(Z_{C_f}+Z_i+R)} \\
&= \frac{\frac{1}{j\Omega C_s}\left(\frac{1}{j\Omega C_f}+\frac{\delta}{\Omega C_f}+R_i+j\Omega L\right)}{\frac{1}{j\Omega C_s}+\frac{1}{j\Omega C_f}+\frac{\delta}{\Omega C_f}+R_i+j\Omega L} \\
&= -\frac{1}{1+j\frac{2Q\Delta\Omega}{\Omega}}\frac{Q}{\Omega C_S}\left[\frac{C_f}{C_s+C_f}+\frac{j}{Q}\right] \\
&\approx -\frac{\mathbb{R}}{1+j\frac{2Q\Delta\Omega}{\Omega_0}}\left(\frac{C_f}{C_s+C_f}\right)^2
\end{aligned} \tag{13}
$$

Here, the shunt resistance of the resonator is $\mathbb{R} = \Omega L Q$ and $\Delta\Omega = \Omega - \Omega_0$ is the difference in tuner resonant angular frequency compared to its average permittivity value Ω_0 which is a function of the permittivity change ($\Delta\epsilon = \epsilon - \epsilon_0$) around the permittivity associated with Ω_0. Balanced operational performance of the tuner implies the center frequency of the tuner's resonator Ω_0 is set to ω_0. The approximation in Eq. (13) is due to the strength of the quality factor Q and shows that matching the impedance of the resonator toward the cavity is controlled by the ratio $C_f/(C_s + C_f)$.

Neglecting losses in the quarter-wavelength transmission line connecting the tuner to the cavity, the resonator impedance Z_r is transformed by the standard transmission line equation to give the tuner load impedance Z_L at the connection to the cavity port:

$$
\begin{aligned}
Z_L &= R_L(\epsilon) + jX_L(\epsilon) \approx \frac{Z_0^2}{Z_r} \\
&= Z_0^2\frac{1+jQ\frac{C_s}{C_s+C_f}\frac{\Delta\epsilon}{\epsilon}}{\mathbb{R}\left(\frac{C_f}{C_s+C_f}\right)^2} \\
R_L &= \frac{Z_0^2}{\mathbb{R}}\left(\frac{C_s+C_f}{C_f}\right)^2 \\
X_L &= Z_0^2\Omega_0\frac{C_s^2}{C_f}\frac{\Delta\epsilon}{\epsilon}
\end{aligned} \tag{14}
$$

with $\mathbb{R}/Q = 1/\Omega_0 C$, and where Z_0 is the characteristic impedance of the quarter-wavelength transmission line. Here, the finite derivative of $\Omega^2 = 1/LC$ with respect to C has been used to give the detuning relation

$$
\frac{\Delta\Omega}{\Omega} = -\frac{C_s}{C_s+C_f}\frac{\Delta\epsilon}{2\epsilon_c}. \tag{15}
$$

Given the complex tuner impedance $Z_L = R_L + jX_L$ from above, and the definition of the FOM in Eq. (2), by assuming a symmetric tuning $|\Delta\Omega_{10}| \simeq |\Delta\Omega_{20}|$ and noting that at the extremal points $(2Q\Delta\Omega/\Omega_0)^2 \gg 1$, the tuner FOM at the cavity can be expressed as

$$
\mathrm{FOM} = \frac{\Delta X_{12}}{2\sqrt{R_1R_2}} \approx \frac{C_s}{(C_s+C_f)}Q\frac{\Delta\epsilon_{12}}{2\epsilon_c} = \frac{C}{C_f}Q\frac{\Delta\epsilon_{12}}{2\epsilon_c} \tag{16}
$$

and shows that the FOM depends on the relative strength of the ferroelectric capacitance C_f to the series capacitance C_s and to the quality factor Q of the resonant tuner but is independent of the tuner shunt impedance $\mathbb{R}$.

The FOM can be further simplified, as the quality factor Q can be expressed in terms of circuit quantities; taking the resonator resistance as parameterized in terms of the ferroelectric material and coaxial modeling of the conductor losses, the quality factor of the tuner Q of the resonator segment of the tuner is

$$
Q = \frac{1}{\Omega_0 CR} = \frac{1}{\Omega_0 C\left(\frac{\delta}{\Omega_0 C_f}+R_i+2R_B\right)} \tag{17}
$$

so that the FOM of Eq. (16) is independent of the series capacitance. As a cross-check, it is noted that if it is assumed the Q of the resonator segment is solely due to the ferroelectric material loss and all conductor losses are neglected, Eq. (16) is reduced to the FOM of the pure ferroelectric as given by Eq. (4).

Finally, with this circuit parametrization, the tuning range between the two permittivity end points can be calculated from the reactance values, and using Eqs. (3) and (14) giving

$$\Delta\omega_{12} = \frac{\omega_0}{2Q_e}\frac{(X_1 - X_2)}{Z_0} = \frac{\omega_0^2 Z_0}{2Q_e}\frac{C_s^2}{C_f}\frac{\Delta\epsilon_{12}}{\epsilon_c}. \tag{18}$$

Having developed the FOM parametrization in terms of equivalent circuit parameters, the circuit parameters can be chosen using procedures described in the next two subsections.

B. Determination of Q_e and the series capacitor

At this stage, the tuner has been defined and the framework for optimization established, but the coupling of the tuner to the cavity has not been addressed in detail. Optimization of this coupling is crucial for improving the tuner performance, as it impacts the choice of both the series capacitor C_s that sets the coupling of the resonator to the transmission line, and the external quality factor Q_e that sets the coupling of the full tuner system to the cavity. To address this optimization, Eq. (3) can be reexpressed by introducing a tuner specific parameter D

$$D = \frac{X_2 - X_1}{2Z_0} \tag{19}$$

such that D can be optimized based on the reactive power, the frequency, and the number of wafers in the tuner. Then, for a given D, the required tuning range sets the value of Q_e, which in turn, from Eq. (18), sets the optimal capacitance C_s; namely

$$C_s = \sqrt{\frac{DC_f}{\Omega_0 Z_0}\frac{2\epsilon_c}{\Delta\epsilon_{21}}}. \tag{20}$$

Again, the tuner's resonator center frequency must satisfy $\Omega_0 = \omega_0$, thereby ensuring that the tuning range is centered around the cavity frequency. Since the ferroelectric capacitance C_f is determined by the geometry, and Eq. (20) sets the series capacitor C_s, the only adjustment left to establish the required resonance condition of the tuner is the setting of the length of the resonator l_r, the short coaxial segment used to model the tuner inductance. This length l_r is the combined length of the spacers and the wafers, and using the reactance of the tuner segment from Eq. (9) with $\Omega_0^2 = 1/LC$ gives l_r:

$$\tan(\Omega_0 l_r/c) = \frac{1}{\Omega_0 Z_r C}, \tag{21}$$

where C is the total tuner capacitance as given by Eq. (7).

C. Optimization of the figure of merit

To set the optimum tuner design, several details of the resonant tuner remain unspecified; the first of which is the radius of the inner conductor a_r and the related width w of the ferroelectric annulus, $w = r_a - r_i$. These two variables are related through the area of the ferroelectric wafers:

$$A_{\text{opt}} = \pi N_w w(2a_r - w) \tag{22}$$

such that a smaller width w leads to a larger inner conductor radius a_r, implying reduced dissipation in the resonator's copper elements. The choice of actual values depends on the power, frequency, and engineering constraints. It is also noted that the choice of the radii ratio b/a for the transmission line has a minimal effect on the performance of the tuner and has been taken as $b/a = 2$ in this work.

The second optimization is the choice of D and b_r, but as D (which determines C_s) and the ratio $\theta \equiv b_r/a_r$ cannot be chosen independently, a simultaneous optimization of both must be made. The existence of an optimal value for θ can be understood by inspecting the denominator of the tuner quality factor Q in Eq. (17). In order to maximize Q, $R_i + 2R_B$ must be minimized, and with explicit expressions for Z_r, α, and l_r from Eq. (21), the denominator can be reexpressed as a function of θ and powers of $\log(\theta)$. Indeed, the optimization of Q simplifies to a minimization of the following function of θ

$$R_i + 2R_B \propto H\frac{1 + \theta^{-1}}{\log(\theta)} + \log(\theta), \tag{23}$$

where $H = H(\Omega, C, a_r)$ is a tuner specific parameter

$$H(\Omega, C, a_r) \equiv \frac{\pi c}{2\Omega_0^2 C a_r \eta}. \tag{24}$$

Similarly, the existence of an optimal value of D becomes clear from Eq. (20): Larger D increases C_s and thus C, leading to a shorter l_r, implying lower inductor losses. On the other hand, if the dissipation in the quarter-wavelength transmission line is considered, one can show that the FOM at the cavity port is maximized when D approaches $D = 1$. These two competing trends lead to an optimal value of D, as shown in Fig. 4(b) for a 1 MVAR tuner. For a 100 kVAR tuner, D stays between 1 and 3.

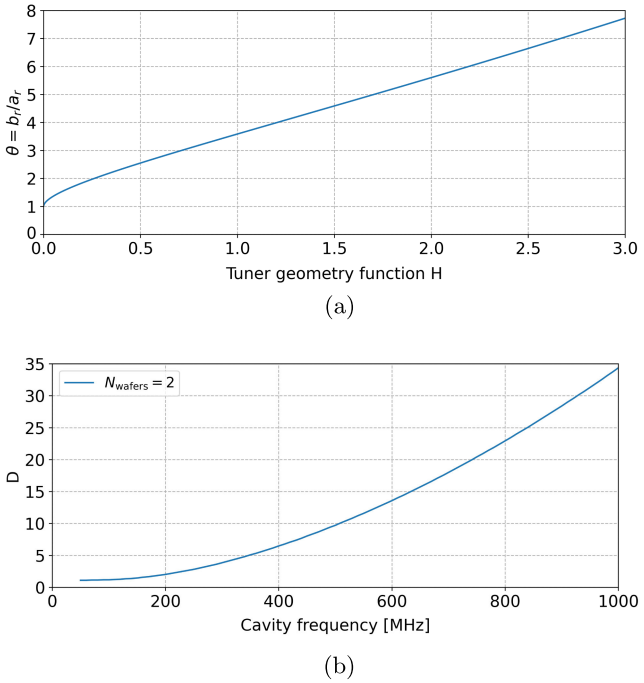

FIG. 4. Optimization of the wafer aspect ratio geometry b_r/a_r and operation point D. (a) The optimum ratio $\theta = b_r/a_r$ as a function of H. (b) The optimum D at 1 MVAR and two wafers as a function of frequency.

Given that H has an implicit dependence on D, it is clear that the optimization of D and b_r/a_r must be done simultaneously, and in this work, has been done numerically.

IV. DISCUSSION AND PERFORMANCE CURVES

The tuner performance for an optimized tuner design can now be evaluated in terms of the tuner FOM as a function of cavity frequency, and power dissipated in the tuner, and Fig. 5 shows the frequency dependency of the optimized FOM for reactive powers of 100 kVAR and 1 MVAR, with the different curves shown corresponding to the number of stacked ferroelectric wafers. This allows the reader to quickly estimate the achievable performance of a particular tuner and match the design to the use case requirements. Given the detailed optimization discussed above, it is noted that the following design choices were made in order to generate Fig. 5: (i) The ferroelectric wafer geometry aspect ratio is adjusted as per Eq. (6), for each given frequency and power. The annulus width is set at 1 mm for the low power case and 3 mm for the high-power case. (ii) The series capacitor is set using Eq. (20). (iii) The resonator length l_r is set using Eq. (21). (iv) The outer radius r_f of the ferroelectric is equal to the radius of the spacers a_r. (v) The quarter-wavelength transmission line to the cavity has dimensions $a = a_r$ and $b = 2a$.

It is observed that the low frequency range for each value of N_w is truncated by a requirement that the length of the resonator l_r does not exceed $\lambda/8$, so to avoid issues with the nonlinear term in the resistance R_i [see Eq. (10)]. Similarly, the high frequency range is truncated at the point where l_r is less than the minimum length of the wafer spacers. In Fig. 5, a 0.5 cm long spacer is assumed for the two-wafer case and 1 cm long spacers for the four and six wafer designs, which limit the reactive power and hence the FOM at the higher frequency end of the curves.

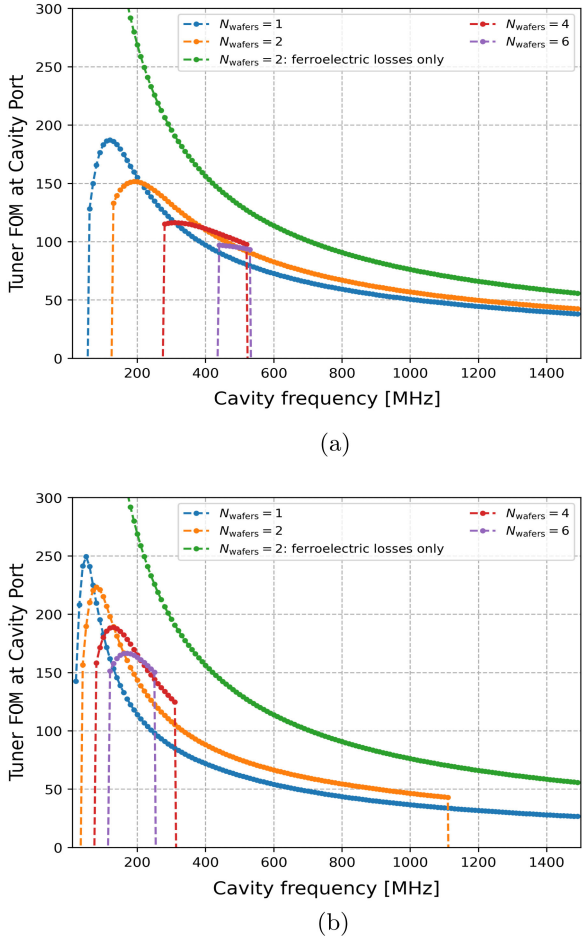

FIG. 5. (a) Tuner FOM for 100 kVAR reactive power input and ferroelectric wafer 1 mm width. (b) Tuner FOM for 1 MVAR reactive power input and ferroelectric wafer 3 mm width. The figure of merit of the tuner (as seen at the cavity port) as a function of frequency for two different reactive power levels. In each case, the design includes optimizations described in the text.

In addition, the function H has a strong dependence on frequency and tuner power (through a_r), and for low frequency and low power designs, H (and thus θ) becomes unreasonably large. At large values of θ, the frequency of the first coaxial resonator modes drop below the operating frequency which could cause unwanted mode competition. For the example shown in Fig. 6, this occurs at $\sim\theta = 7$. Consequently, the results shown in Fig. 5(a) include a limit of $H < 3$, and the FOM at low frequencies is not fully optimized, as is evident from a comparison with Fig. 5(b).

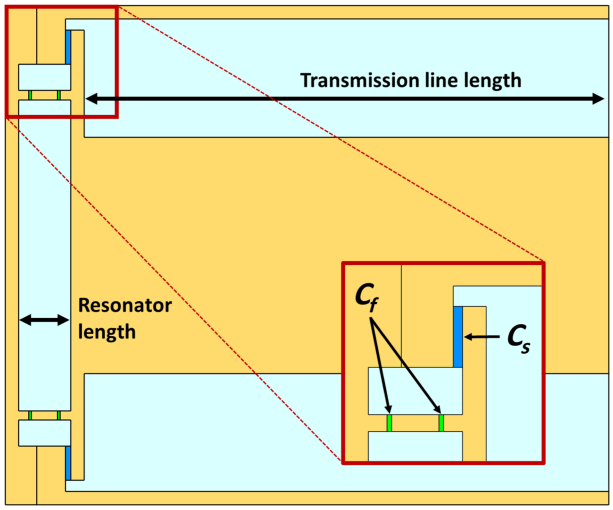

FIG. 6. CST model of tuner design showing the implementation of C_f and C_s. Light blue represents vacuum space.

As these figures represent tuner performance over a considerable frequency range, ferroelectric wafer configurations, and widely different reactive power levels, some immediate conclusions may be drawn. For tuner designs with in-series stacks of ferroelectric wafer geometries, configurations with more than two wafers do not offer a significant advantage in FOM at low reactive power levels; with a four-wafer design, there may be a slight performance benefit at low frequencies, but at the price of added mechanical complication.

The FOM values, following optimization procedures, are relatively high, being of the order of 100 at 100 kVAR reactive power. At the higher reactive power of 1 MVAR, the FOM starts higher at low frequencies, even exceeding 200, but drops fast with increasing frequency.

V. ELECTROMAGNETIC DESIGN PROCEDURE

In order to cross-check the analytical formulas from the previous sections, an assessment of tuner design performance based on detailed modeling and electromagnetic simulation has been performed, using the CST Studio Suite [10] simulation package. The tuner design example is as summarized by the analytically calculated input parameters given in Table I and represents a tuner design comprising two ferroelectric wafers of an annulus shape, capable of sustaining 1.9 MVAR reactive continuous tuning power. An outline of the design is shown in Fig. 6, with the two ferroelectric wafers that comprise the capacitance C_f, and a (nonferroelectric) sapphire annulus as the capacitance C_s shown in the inset of Fig. 6. Implementing C_s in this way also provides a clean way to separate the resonator vacuum and the cavity vacuum. The top part of the resonator shows a break, indicating that it is removable and would be sealed with a vacuum flange. It is noted that this model is not a full mechanical design of a tuner and only a representative model for electromagnetic simulation purposes.

TABLE I. Analytical design parameters used for comparison.

Parameter	Analytical	Units
f_0	400.7948	MHz
U	136	J
Δf	1.1	kHz
A_{opt}/g	1153.7	mm
w	3	mm
Z_0	41.6	Ω
a	45	mm
b	90	mm
a_r	62.71	mm
b_r	72.77	mm
Q_e	3.25	$\times 10^6$

A. Stand alone tuner

To implement the detailed modeling of this high-power tuner design for a 400 MHz cavity, the value of the A_{opt}/g was set to the same value as the analytical model and is defined by the minimum area that can sustain the power dissipated in the material. In addition, the width of the sapphire capacitor C_s was initially set using an electrostatic solver to estimate the capacitance. With these two values set, the model was then generated and simulated, with the tuner geometry as shown in Fig. 6. The permittivity of the ferroelectric material was varied from ϵ_1 to ϵ_2, with the S_{11} response observed for each state. The tuner resonant frequency for each state was evaluated, and then the resonator length was set such that the average of the two end state frequencies was at the cavity frequency, and so that the end states were equally spaced around f_0. A central value of the permittivity that gives this resonance at f_0 can be defined, as shown in Fig. 7, along with the two end state resonances.

B. Attaching the tuner to a cavity

After the dimensions of the tuner had been approximately set, it was attached to a two-cell, 400 MHz cavity as shown in Fig. 8. The cavity had three ports, one for the FRT with Q_e set to the design value from Table I, a fundamental power coupler (FPC) port with $Q_e = 5 \times 10^7$ and a probe port with $Q_e = 5 \times 10^9$. The stand-alone cavity with the three ports, including the FRT port was simulated separately in order to set the values of Q_e, where each port is terminated with its characteristic impedance. The resonant frequency of the three-port cavity was also set to f_0, assumed to be the resonant frequency with no tuner attached.

As per the analytic model, the transmission line length connecting the tuner to the cavity should be exactly $\lambda/4$ in length, though uncertainty in the region where the coaxial

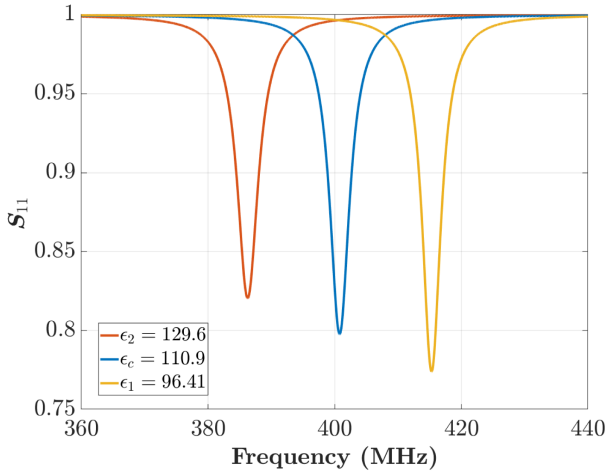

FIG. 7. S_{11} vs frequency for the two end states (ϵ_1, ϵ_2) and a central value of ϵ_c.

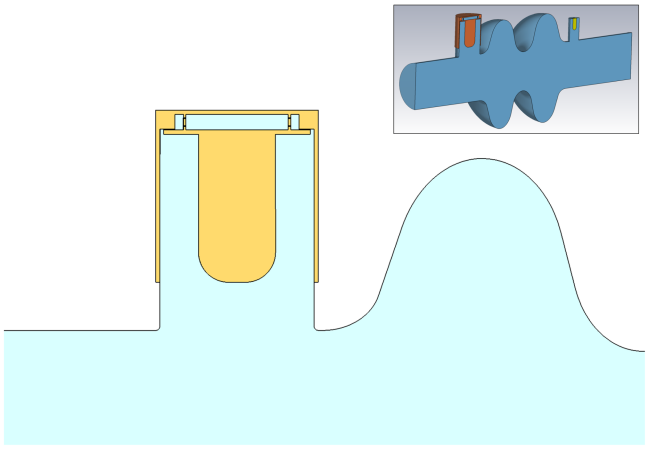

FIG. 8. Detail of tuner attached to two-cell 400 MHz cavity.

line transitions into the cavity means this is difficult to estimate. In order to properly set the transmission line length, the tuning range response as a function of line length was simulated, and the minima of the tuning range used to identify the correct transmission line length for that particular tuner configuration, as shown in Fig. 9. Further, it was found that with the input parameters from the analytical model, the tuning range minima was only 0.97 kHz instead of the 1.1 kHz required. To increase the tuning range without affecting the other tuner parameters, Q_e was adjusted from 3.25×10^6 to 2.95×10^6, bringing the tuning range to 1.1 kHz. Finally, to have a clear comparison quantity for the CST simulation, Q_{FRT} was calculated using the known Q_e of the FPC and probe ports and the measured Q_L using

$$Q_{\mathrm{FRT}} = \frac{1}{\frac{1}{Q_L} - \frac{1}{Q_0} - \frac{1}{Q_{\mathrm{FPC}}} - \frac{1}{Q_{\mathrm{probe}}}}. \tag{25}$$

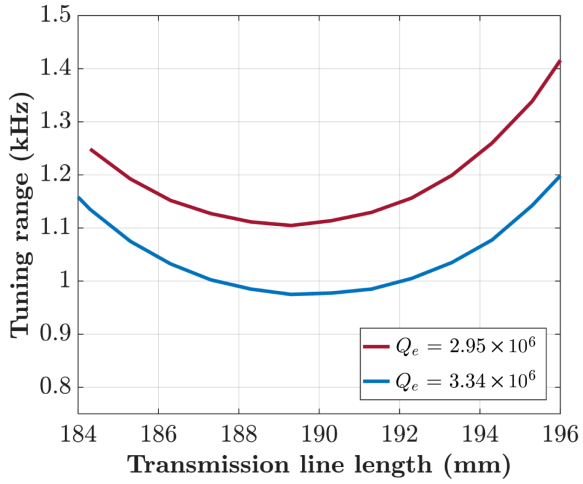

FIG. 9. Tuning range vs transmission line length for two values of Q_e.

The FOM was then evaluated using the average Q_{FRT} of the two end states and the tuning range, Δf:

$$\mathrm{FOM} = \frac{4\pi \Delta f \overline{Q_{\mathrm{FRT}}}}{\omega_0} \tag{26}$$

and the 12% reduction in Q_e was expected to cause a similar reduction in the measured Q_{FRT} and hence the FOM.

C. Final tuning

Final fine adjustment of parameters to center the end states around the cavity frequency f_0 while maintaining the required tuning range was performed using the in-built CST optimization framework, with the following optimization objectives: (A) $\Delta f = |f_1 - f_2| = 1.1$ kHz and (B) $\delta_f = |f_0 - (f_1 + f_2)/2| < 0.01$ kHz where f_1 and f_2 are the frequencies of the two end states. Clearly, objective A is the tuning range requirement, while objective B enforces the tuning range to be centered on the cavity frequency with no tuner attached, f_0.

The inputs of the optimization were the geometry of the sapphire annulus making up C_s and the tuner resonator length, l_r, and the comparison of the analytical and CST simulation results is shown in Table II. Excellent agreement is seen between the analytical capacitance values and those estimated using an electrostatic solver. The length of the resonator also shows good agreement, indicating that the analytical model predicts the frequency of the tuner resonator well. The final S parameters, as observed through the FPC port, are shown in Fig. 10. It is noted that the analytical model predicts a larger value of ΔX_{12} than is obtained in CST for the particular tuner configuration. This implies a need to reduce Q_e in the CST model, in order to increase the tuning range, and correspondingly, leads to a reduction in the CST values of both Q_{FRT} and the FOM. If Q_e is left unchanged, Q_{FRT} can be increased to 3.1×10^7,

TABLE II. Comparison of analytical and optimized CST values for a 400 MHz tuner design.

Parameter	Analytical	CST	Units
Δf	1.1	1.1	kHz
C_f	551.9	563.3	pF
C_s	578.3	584	pF
l_r	18.39	18.05	mm
$\overline{Q_{\mathrm{FRT}}}$	3.18	2.38	$\times 10^7$
FOM	81.6	65.3	…
δf_1	550.3	554.8	Hz
δf_2	549.8	550	Hz
Q_e	3.25	2.95	$\times 10^6$

which is more in line with the analytic model, but the tuning range is reduced to 0.93 kHz. Finally, including all the loss mechanisms that are not included in the analytical model, such as extra lengths of copper and the losses in the sapphire used to make C_s, further reduces Q_{FRT} by ≈4%.

The same methodology was also applied to an 800 MHz tuner design at a power level of 458 kVAR, with the analytical values presented in Table III and comparison in Table IV. This tuner design was based on a potential use-case for a conceptual FCC-ee booster scenario whereby cavities must be detuned by 1.5 kHz every 3.8 s during injection [12]. For this case, Q_e was not adjusted to compensate for the decreased tuning range compared to the analytical estimate, resulting in a ∼15% reduction in tuning range. The FOM is also much closer to the analytical value, with the ∼13% difference being attributed to extra losses that are not accounted for in the analytical model. The agreement between the analytical and numeric calculations is excellent just as in the 400 MHz case.

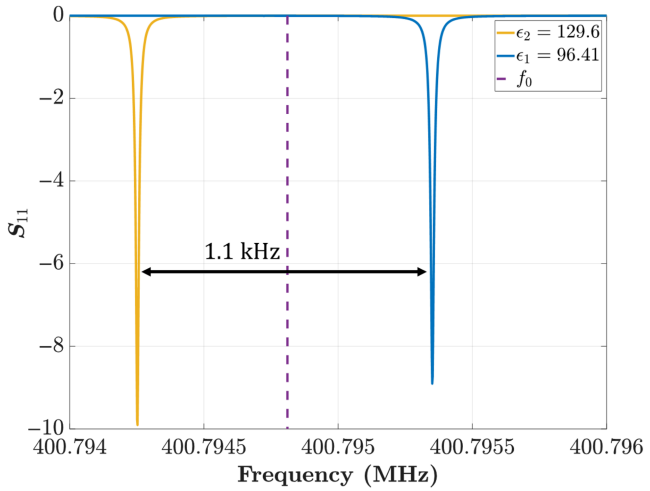

FIG. 10. Final S parameters observed through the FPC port with $Q_e = 5 \times 10^7$.

TABLE III. Analytical design parameters (800 MHz).

Parameter	Analytical	Units
f_0	801.59	MHz
U	24.3	J
Δf	1.5	kHz
A_{opt}/g	483.2	mm
w	2	mm
Z_0	41.6	Ω
a	32.5	mm
b	65	mm
a_r	39.5	mm
b_r	45.5	mm
Q_e	4.9	$\times 10^6$

TABLE IV. Analytical vs CST design (800 MHz).

Parameter	Analytical	CST	Units
Δf	1.5	1.3	kHz
C_f	230.9	239.5	pF
C_s	268	280.6	pF
l_r	10.8	8.59	mm
$\overline{Q_{\mathrm{FRT}}}$	3.28	3.1	$\times 10^7$
FOM	56.6	49.3	…
δf_1	755	737	Hz
δf_2	745	548	Hz

VI. SUMMARY

This paper presents a methodology for designing and optimizing a coaxial type resonant ferroelectric fast reactive tuner operating at high average reactive power levels over a broad range of operating frequencies. The tuner, as represented by the schematic of Fig. 1, comprises a ferroelectric capacitor, which has N_W wafers in series, separated by spacers that provide a bias voltage and cooling. A particular ferroelectric material is used in the design, with material properties taken from the ferroelectric supplier [11].

Given a cavity with known stored energy, operating frequency, and desired tuning range, the reactive power for the tuner is determined. The ferroelectric material properties, together with the frequency and reactive power, determine the minimum area of the ferroelectric wafers that can sustain this power. The choice of ferroelectric ring geometry and sizing then leads to a choice of the radius of the inner conductor of the tuner resonator segment, and the optimization of the FOM leads to specific choices for the coupling capacitor C_s and the radius of the resonator's outer conductor. Depending on the frequency and reactive power requirements, Fig. 4 then gives the preferred number of ferroelectric capacitors in series N_w.

To illustrate the application of this design methodology to a particular case, two examples are considered, with analytic modeling of optimized tuner design compared to full electromagnetic simulation of three-dimensional

geometry. The first is a case of a very demanding tuner for a two-cell 400 MHz cavity with the significant reactive power level of $\Delta P_{\text{reactive}} = 1.9$ MVAR. The second is a higher frequency (800 MHz) tuner with a reactive power level of 458 kVAR. The agreement is excellent for both examples, proving that the analytical model provided gives an accurate set of initial parameters before starting on the detailed 3D electromagnetic design.

ACKNOWLEDGMENTS

This work is in part supported through the Innovate for Sustainable Accelerating Systems (iSAS) programme funded through the European Commission's Horizon Europe Research and Innovation programme under Grant Agreement No. 101131435. I. B.-Z. acknowledges support under the CERN Visiting Scientist program.

DATA AVAILABILITY

The data are not publicly available. The data are available from the authors upon reasonable request.

[1] S. Y. Kazakov, S. Shchelkunov, V. Yakovlev, A. Kanareykin, E. Nenasheva, and J. Hirshfield, Fast ferroelectric phase shifters for energy recovery linacs, Phys. Rev. ST Accel. Beams **13**, 113501 (2010).

[2] Y. M. Pischalnikov, S. Kazakov, T. N. Khabiboulline, V. P. Yakovlev, and A. V. Burov, Fast electrically-controlled ferroelectric tuners for rf cavities, Technical Report, Fermi National Accelerator Laboratory (FNAL), Batavia, IL, Report No. FERMILAB-TM–2730-AD-TD, 2020.

[3] N. C. Shipman *et al.*, Ferro-electric fast reactive tuner applications for SRF cavities, in *Proceedings of the 12th International Particle Accelerator Conference (IPAC2021)* (JACoW, Geneva, Switzerland, 2021), pp. 1305–1310.

[4] A. Kanareykin, S. Kazakov, A. Kozyrev, E. Nenasheva, and V. Yakovlev, Ferroelectric based high power tuner for l-band accelerator applications, in *Proceedings of the 4th International Particle Accelerator Conference (IPAC 2013), Shanghai, China* (JACoW, Geneva, Switzerland, 2013), WEPWO082, pp. 2486–2488, https://jacow.org/IPAC2013/papers/WEPWO082.pdf.

[5] I. Ben-Zvi and N. Shipman, High power fast frequency modulation, arXiv:2502.13312.

[6] S. Kazakov, S. Shchelkunov, V. Yakovlev, A. Kanareykin, E. Nenasheva, J. Hirshfield, T. Khabiboulline, H. Hahn, and E. Choi, Fast high-power microwave ferroelectric phase shifters for accelerator application, AIP Conf. Proc. **1086**, 477 (2009).

[7] I. Ben-Zvi, G. Burt, A. Castilla, A. Macpherson, and N. Shipman, Conceptual design of a high reactive-power ferroelectric fast reactive tuner, Phys. Rev. Accel. Beams **27**, 052001 (2024).

[8] I. Ben-Zvi, A. Castilla, A. Macpherson, and N. Shipman, High-power ferro-electric fast reactive tuner, arXiv:2109.06806.

[9] MapleSoft: Maple is a Trademark of Waterloo Maple Inc., Maple, https://www.maplesoft.com (2024).

[10] Dassault Systèmes, CST Studio Suite, R2024x, https://www.3ds.com/products-services/simulia/products/cst-studio-suite/ (2024).

[11] A. Kanareykin, E. Nenasheva, S. Karmanenko, A. Dedyk, and V. Yakovlev, Low-loss ferroelectric for accelerator applications, in *Proceedings of the 2005 Particle Accelerator Conference* (IEEE, New York, 2005), pp. 4305–4307.

[12] FCC Collaboration *et al.*, FCC-ee: The lepton collider: Future circular collider conceptual design report volume 2, Eur. Phys. J. Special Topics **228**, 261 (2019).